Catalysis
Science & Technology

Dynamic Article Links

Cite this: *Catal. Sci. Technol.*, 2011, **1**, 669–674

www.rsc.org/catalysis

PAPER

Effect of Fe doping on the catalytic performance of $CuO–CeO_2$ for low temperature CO oxidation

Shimei Ma,[a] Guanzhong Lu,*[ab] Yuexin Shen,[a] Yun Guo,[a] Yanqin Wang[a] and Yanglong Guo[a]

Received 9th February 2011, Accepted 30th March 2011
DOI: 10.1039/c1cy00049g

$Cu_1Ce_8Fe_x$–O catalysts for low temperature CO oxidation were prepared by an improved citrate sol–gel method with incorporation of thermal treatment under N_2, and characterized by the nitrogen adsorption–desorption, XRD, CO pulse experiments, CO-TPR and CO-TPD. When $x = 1$, the $Cu_1Ce_8Fe_1$–O catalyst shows higher catalytic activity for CO oxidation, and the reaction temperature for 90% CO conversion (T_{90}) is only 50 °C. The presence of Fe in $Cu_1Ce_8Fe_1$–O can improve the catalytic activity for CO oxidation, which results from its higher surface area, smaller crystalline size, higher activity and larger amounts of surface oxygen species.

1. Introduction

As a toxic gas, CO exists widely in the utilization processes of any fuel burning appliance, vehicles, tools with fuel or other devices, and in many industrial processes, causing environmental pollution. Catalytic oxidation is one of the most effective methods to abate CO by converting CO to CO_2. So far, the catalysts used for CO oxidation include supported noble metal catalysts (*e.g.* Pt, Ru, and Au),[1–6] transition metal oxides (*e.g.* CuO, Cu–Mn–O, Co_2O_3)[7,8] and others. Although noble metal catalysts have high activity, their high cost and poor stability limits their application.[6] Therefore, there is a strong demand to develop a novel, thermally stable and low cost catalyst for CO oxidation, and especially for CO oxidation at low temperature. It has been reported that the CeO_2 catalyst shows great oxygen storage/release properties and high activity for CO oxidation, and its activity can be improved significantly by adding other transition metal oxides, such as CuO,[9] for instance, over the Ce_7Cu_3–O catalyst T_{10} (the reaction temperature for 10% CO conversion) reached 76 °C. It has been reported that the CeO_2–CuO catalyst is equal or superior to platinum catalysts for the preferential oxidation of CO in excess hydrogen,[10–12] but its activity is relatively low compared with nano-gold catalysts.

Iron oxide has been used in many catalytic processes, such as the water–gas shift reaction, the oxidation of phenol in the liquid phase,[13,14] and selective removal of CO in methanol reformed gas.[15–19] Iron oxide supported noble metal catalysts have been demonstrated to be very effective for low-temperature CO oxidation. Haruta *et al.*[20] firstly developed the Au–Fe_2O_3 catalyst for CO oxidation at room temperature. Deng *et al.*[21] successfully prepared ferric hydroxide supported 4 wt% Pd catalyst, over which the complete oxidation of CO could be achieved at temperatures as low as −15 °C. It was reported that as a large amount of oxygen can adsorb on FeO_x, in the Pt–FeO_x catalyst FeO_x acting as an oxygen supply can provide sufficient active oxygen species for CO oxidation.[22] Cao *et al.*[23] reported that CuO–Fe_2O_3 composite oxide catalysts with high surface area exhibited high catalytic activity and stability for low-temperature CO oxidation. Sirichaiprasert *et al.*[24] reported that the Cu–Fe–Ce–O composite oxide catalyst prepared by urea–nitrate combustion and a single-step citrate method was used in the selective oxidation of CO to CO_2 in a hydrogen stream, and using the $Cu_{0.15}Ce_1Fe_{0.5}$–O catalyst 50% CO conversion was obtained at ~115 °C. We have found that adding an appropriate amount of Fe in CeO_2 can form $Ce_{1-x}Fe_xO_{2-\delta}$ solid solutions ($x \leq 0.2$) and the $Ce_{0.9}Fe_{0.1}O_2$ solid solution presents higher catalytic performance for CH_4 and CO oxidation.[25] Based on the research results reported, we have developed the Cu–Fe–Ce–O catalyst for low temperature CO oxidation, and are trying to improve its catalytic performance to satisfy the demands of purifying CO in air pollution, which has barely been reported.

Herein, the Cu–Ce–Fe–O composite oxide catalyst was prepared by the citrate sol–gel method, which shows the high catalytic activity for CO oxidation (its T_{90} is 50 °C). The influence of Fe doping on the properties of the CuO–CeO_2 composite oxide was investigated by means of the nitrogen adsorption–desorption, XRD, CO pulse and CO-TPR and CO-TPD techniques, and the role of Fe in the Cu–Ce–O catalyst was discussed.

[a] *Key Laboratory for Advanced Materials and Research Institute of Industrial Catalysis, East China University of Science and Technology, Shanghai 200237, P. R. China. E-mail: gzhlu@ecust.edu.cn; Fax: +86-21-64253824*
[b] *Research Institute of Applied Catalysis, Shanghai Institute of Technology, Shanghai 200235, P. R. China*

2. Experimental

2.1 Catalyst preparation

The $Cu_1Ce_8Fe_1$–O catalyst was prepared by the citrate sol–gel method. A mixture of $Ce(NO_3)_3{\cdot}6H_2O$, $Cu(NO_3)_2{\cdot}3H_2O$ and $Fe(NO_3)_3{\cdot}9H_2O$ with a molar ratio of Cu : Ce : Fe = 1 : 8 : 1 was dissolved in de-ionized water. The obtained solution was stirred at 90 °C until a viscous gel was formed. Then this gel was dried at 100 °C overnight to form a spongy material of $Cu_1Ce_8Fe_1$–O citrate precursor, and finally calcined in N_2 at 600 °C for 2 h, and then calcined in air at 400 °C for 2 h. Changing the amount of $Fe(NO_3)_3{\cdot}9H_2O$ in the synthesis solution, a series of $Cu_1Ce_8Fe_x$–O catalysts with different Fe amounts were prepared, in which x = 0.5–2. The compositions of the catalysts were determined by ICP–AES technology (Varian 710), and the results are shown in Table 1 and are similar to the compositions of the synthesis solutions. The samples of CeO_2, Fe_2O_3 and CuO were also prepared with the same method above.

2.2 Catalyst characterization

Powder X-ray diffraction patterns were recorded on a Rigaku D/max 2250VB/PC diffractometer with Cu-Kα radiation (λ = 1.5406 Å) at scanning rate of 6° min^{-1}. The average crystalline size was determined by the Scherrer formula based on the CeO_2 (111) diffraction peak broadening. N_2 adsorption–desorption isotherms were measured at −196 °C on a NOVA 4200e surface area and pore size analyzer. The samples were outgassed at 180 °C for 4 h before testing. The Brumauer–Emmett–Teller (BET) method was used to calculate the specific surface areas of samples.

The CO temperature-programmed reduction (CO-TPR) was conducted in a conventional flow system with a quartz tube reactor packed 100 mg sample. Before testing, the catalyst was pre-treated at 400 °C for 40 min in the mixture gas of 20% O_2/He (50 ml min^{-1}) and then cooled down to room temperature, and swept with He for 1 h. CO-TPR was run in 5% CO/He flow (50 ml min^{-1}) at a heating rate of 10 °C min^{-1} from room temperature to 500 °C. The effluent gas was monitored by on-line quadrupole mass spectrometry (MS, IPC 400, INFICON Co. Ltd.).

The CO pulse experiments were conducted on the quartz tube reactor and the effluent gas was monitored by on-line quadrupole MS. 100 mg catalyst was used and pretreated at 400 °C for 40 min in the mixture gas of 20% O_2/He (50 ml min^{-1}), and then cooled down to 60 °C in He atmosphere. After the system was reached the equilibrium, 35.6% CO/Ar was pulsed into the reactor system at an interval of 30 s with a loop volume of 73.7 μl.

Table 1 Compositions of the catalysts measured by an ICP–AES instrument

Catalyst	Cu : Ce : Fe (mol)
$Cu_1Ce_8Fe_{0.5}$–O	1 : 7.8 : 0.49
$Cu_1Ce_8Fe_{0.95}$–O	1 : 8.0 : 0.91
$Cu_1Ce_8Fe_1$–O	1 : 7.9 : 0.97
$Cu_1Ce_8Fe_{1.05}$–O	1 : 7.8 : 1.02
$Cu_1Ce_8Fe_2$–O	1 : 7.9 : 2.05

The CO-TPD experiments were performed in a quartz tube reactor at atmospheric pressure. 100 mg catalyst was pre-treated in the mixture gas of 20% O_2/He (50 ml min^{-1}) at 400 °C for 40 min to remove the surface impurities. After the reactor was cooled down to room temperature, 35.6% CO/Ar (20 ml min^{-1}) was introduced through the catalyst till the saturated adsorption, then He was purged instead of CO/Ar and was heated from room temperature to 400 °C at a heating rate of 10 °C min^{-1}. The effluent gas was monitored by an on-line quadrupole MS.

2.3 Testing of catalytic activity

The catalytic activities of all catalysts for CO oxidation were carried out in a quartz tube reactor packed 0.20 g catalyst at atmospheric pressure. The reagent gas was consisted of 1% CO–20% O_2/N_2 and the flow rate was 50 ml min^{-1}. A space velocity (SV) was 15 000 ml $(g\ h)^{-1}$. The reactants and products are analysed by on-line GC with flame ionization detector (FID).

3. Results and discussion

3.1 Testing of catalytic activity

Fig. 1 shows the catalytic performances of CeO_2, Fe_2O_3, CuO, Cu_1Ce_9–O and $Cu_1Ce_8Fe_1$–O for CO oxidation, and T_{10} (the reaction temperature for 10% CO conversion), T_{50} and T_{90} are shown in Table 2. It can be seen that CO conversion on CeO_2 is the lowest, and the activity of CuO is similar to that of Fe_2O_3, for instance, T_{90} (the reaction temperature for 90% CO conversion) on the CuO and Fe_2O_3 catalysts is 150 °C and 160 °C, respectively. When CeO_2 is doped by CuO to form Cu_1Ce_9–O mixed oxides, its activity can be improved significantly, for example, T_{90} reaches to 70 °C. After Fe doping into Cu_1Ce_9–O, its catalytic activity can be further increased, T_{90} reaches to 50 °C.

Fig. 2 shows the effect of Fe amount on the catalytic activities of $Cu_1Ce_8Fe_x$–O catalysts for CO oxidation. When x = 1, the $Cu_1Ce_8Fe_1$–O catalyst behaves the best activity, T_{10} = 10 °C, T_{50} = 30 °C and T_{90} = 50 °C. When $x > 1$ or $x < 1$, the activities of catalysts declined obviously, compared with the activity of the $Cu_1Ce_8Fe_1$–O catalyst; even if x = 0.95 or x = 1.05, the catalytic activities of catalysts are lower than that of the $Cu_1Ce_8Fe_1$–O catalyst.

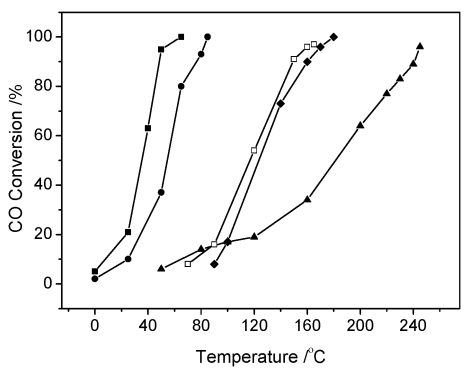

Fig. 1 Catalytic activities of CeO_2 (▲), Fe_2O_3(◆), CuO (□), Cu_1Ce_9–O (●) and $Cu_1Ce_8Fe_1$–O (■) for CO oxidation.

Table 2 BET surface areas (SA), crystallite sizes (d) and CO oxidation activities over CeO_2, Cu_1Ce_9–O and $Cu_1Ce_8Fe_1$–O

Catalyst	T_{10} (°C)	T_{50} (°C)	T_{90} (°C)	d (nm)	SA ($m^2\ g^{-1}$)
CeO_2	70	180	240	7.8	25
Cu_1Ce_9–O	20	50	70	7.4	120
$Cu_1Ce_8Fe_1$–O	10	30	50	5.2	164

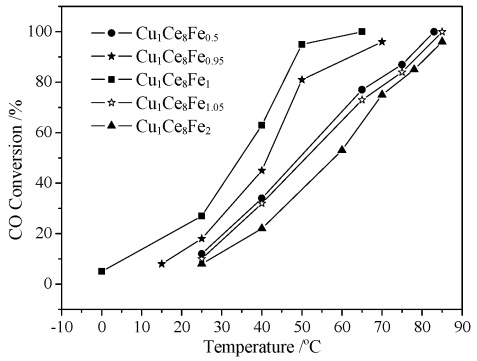

Fig. 2 Catalytic activities of $Cu_1Ce_8Fe_{0.5}$–O (●), $Cu_1Ce_8Fe_{0.95}$–O (★), $Cu_1Ce_8Fe_1$–O (■), $Cu_1Ce_8Fe_{1.05}$–O (☆) and $Cu_1Ce_8Fe_2$–O (▲) for CO oxidation.

The stability of $Cu_1Ce_8Fe_1$–O for CO oxidation has been tested in 1% CO–20% O_2/N_2 at 65 °C, and the results are shown in Fig. 3. The results show that 100% CO conversion over $Cu_1Ce_8Fe_1$–O can be maintained for ~2 h, and then the CO conversion reduces gradually to 90% after which it hardly varied within 90 h.

The above results show that, doping with the appropriate amount of Fe in the Cu_1Ce_8–O catalyst can obviously improve its catalytic activity and increase the CO conversion; the $Cu_1Ce_8Fe_1$–O catalyst exhibits higher stability for CO oxidation.

3.2 XRD and BET surface area

The XRD patterns of the catalysts are shown in Fig. 4. It can be found that no diffraction peaks of CuO and Fe_2O_3 are observed in the XRD patterns of Cu_1Ce_9–O and $Cu_1Ce_8Fe_1$–O, indicating that CuO and Fe_2O_3 are finely dispersed in the catalysts to form

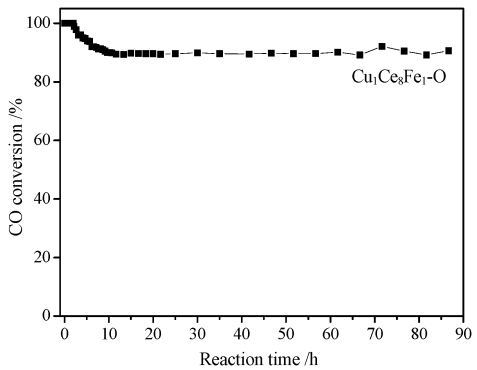

Fig. 3 CO conversion as a function of the reaction time over the $Cu_1Ce_8Fe_1$–O catalyst at 65 °C. (1% CO–20% O_2/N_2 balance, WHSV 15000 ml $(gh)^{-1}$).

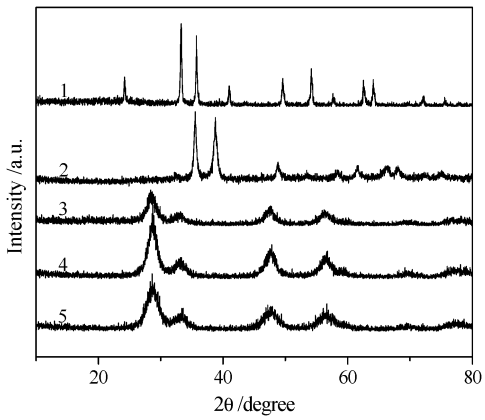

Fig. 4 XRD patterns of (1) Fe_2O_3, (2) CuO, (3) CeO_2, (4) Cu_1Ce_9–O and (5) $Cu_1Ce_8Fe_1$–O.

a solid solution or their crystal size is too small to be detected. The crystalline size of Cu_1Ce_9–O is 7.4 nm, which is smaller than that of pure CeO_2 (7.8 nm). After doping Fe into Cu_1Ce_9–O, its crystalline size further diminishes, for instance, the crystalline size of $Cu_1Ce_8Fe_1$–O is only 5.2 nm, resulting in its highest catalytic activity. It can also be seen that the diffraction peaks of CeO_2 in the XRD patterns of Cu_1Ce_9–O and $Cu_1Ce_8Fe_1$–O hardly shift but rather its diffraction peaks intensify in a comparable way to that of pure CeO_2, which has rarely been reported. Fig. 5 shows the TEM images of CeO_2, Cu_1Ce_9–O and $Cu_1Ce_8Fe_1$–O samples. It can be seen that after doping Cu or Cu–Fe–O into CeO_2, the crystalline sizes of sample become obviously smaller, and are similar results obtained by XRD (Table 2).

The data in Table 2 show that the BET surface area of CeO_2 is 25 $m^2\ g^{-1}$, and the surface area of Cu_1Ce_9–O reaches 120 $m^2\ g^{-1}$. After doping Fe_2O_3 into Cu_1Ce_9–O, the BET surface area of $Cu_1Ce_9Fe_1$–O further increases to 164 $m^2\ g^{-1}$. It is very obvious that, the higher surface area of $Cu_1Ce_9Fe_1$–O compared to that of Cu_1Ce_9–O and CeO_2 is one of the reasons that $Cu_1Ce_9Fe_1$–O possesses the excellent catalytic performance, because the catalyst with higher surface area can provide more active sites to enhance its catalytic activity.[26,27]

3.3 CO-TPR

The CO-TPR (CO_2 produced) profiles of CuO, Fe_2O_3, CeO_2, Cu_1Ce_9–O and $Cu_1Ce_9Fe_1$–O samples are shown in Fig. 6, in which the curves of CO_2 produced are the same as the curves of CO consumption. The results show that there is a broad and asymmetric peak of CO_2 desorption at 160–500 °C (top temperature, 255 °C) in the CO-TPR profile of CuO, which can be assigned to direct reduction of CuO to metallic copper.[28,29] In the CO-TPR profile of Fe_2O_3 there is a CO_2 peak at ~315 °C and a broad band at >350 °C, and in the CO_2 desorption curve of CeO_2, no obvious desorption peak of CeO_2 can be observed at <500 °C, which indicates that CeO_2 is hardly reduced by CO at <500 °C. It can also be seen that there are two CO reduction peaks at 103 °C and 182 °C in the CO-TPR profile of Cu_1Ce_9–O, and the former should be assigned to reduction of the surface oxygen species,[30,31] and the latter corresponds to the reduction of lattice oxygen.

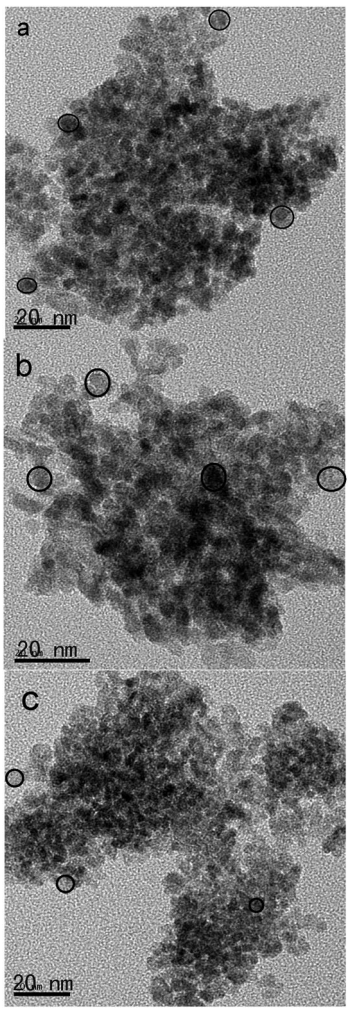

Fig. 5 TEM images of (a) CeO_2, (b) Cu_1Ce_9–O, and (c) $Cu_1Ce_8Fe_1$–O.

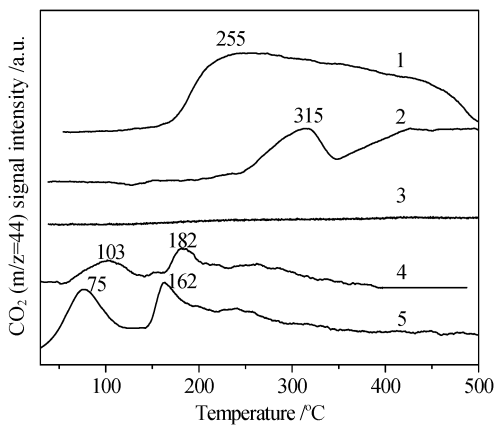

Fig. 6 CO_2 (m/z = 44) evolution curves in CO-TPR-MS of (1) CuO, (2) Fe_2O_3, (3) CeO_2, (4) Cu_1Ce_9–O and (5) $Cu_1Ce_8Fe_1$–O.

After Cu_1Ce_9–O is modified with Fe, its reduction property is promoted obviously, for instance, the first reduction peak falls down from 103 °C to 74 °C and second reduction peak falls from 182 °C to 162 °C, indicating that the surface oxygen and lattice oxygen of $Cu_1Ce_8Fe_1$–O are more active than that of Cu_1Ce_9–O. The fact that the peak area of low temperature CO reduction of $Cu_1Ce_8Fe_1$–O is larger than that of Cu_1Ce_9–O indicates that $Cu_1Ce_8Fe_1$–O possesses a much larger amount of surface oxygen species. The results above may deduce that more highly active and large amounts of the surface oxygen species are one of the main reasons for $Cu_1Ce_8Fe_1$–O displaying high catalytic activity and better reducibility by CO.

CO-TPR of $Cu_1Ce_8Fe_1$–O was repeatedly measured three times and the results are shown in Fig. 7. The results exhibit that the CO-TPR profiles of $Cu_1Ce_8Fe_1$–O obtained the second and third time are similar to that of the fresh catalyst, indicating that the reduction temperature of $Cu_1Ce_8Fe_1$–O is hardly changed after redox cycles.

3.4 CO pulse experiments

The surface oxygen properties of $Cu_1Ce_9Fe_1$–O and Cu_1Ce_9–O were investigated by the CO pulse experiment, and the results are shown in Fig. 8. It can be seen that the intensities of CO signals (m/z = 28) at the first several pulses on $Cu_1Ce_9Fe_1$–O are much lower than that on Cu_1Ce_9–O, as the red line indicates. The amounts of CO consumption on $Cu_1Ce_9Fe_1$–O and Cu_1Ce_9–O were measured and are 3.13 mmol g^{-1}_{cat} and 2.27 mmol g^{-1}_{cat}, respectively. These results indicate that more CO molecules was reduced by the active oxygen species of $Cu_1Ce_9Fe_1$–O and further supports the results of CO-TPR above, that is, $Cu_1Ce_8Fe_1$–O has a larger amount of the active oxygen species than Cu_1Ce_9–O.

3.5 CO-TPD

The CO-TPD technique was used to investigate the CO adsorption on the catalysts. As shown in Fig. 9, there are three peaks located at 120 °C, 160 °C and 192 °C in the CO-TPD (CO_2 produced) profile of Cu_1Ce_9–O, indicating that there are three kinds of CO adsorption sites on its surface. Similarly, there are also two larger peaks of CO_2 desorption at 84 °C and 154 °C in the CO-TPD profile of $Cu_1Ce_8Fe_1$–O. Compared with that of Cu_1Ce_9–O, the desorption peaks of CO_2 in the CO-TPD profile of $Cu_1Ce_8Fe_1$–O shift to lower temperature, which implies that CO adsorbed on $Cu_1Ce_8Fe_1$–O is oxidized more easily by its surface oxygen

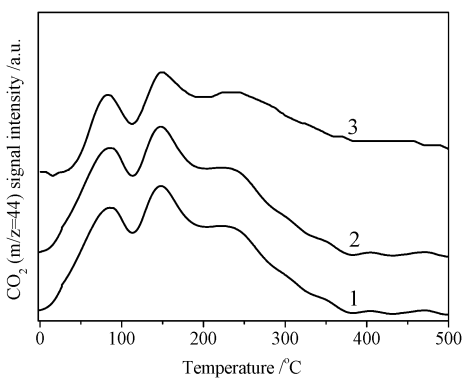

Fig. 7 The CO_2 (m/z = 44) curves in CO-TPR-MS of $Cu_1Ce_8Fe_1$–O (1), second run (2) (after first testing of CO-TPR, this catalyst was treated at 500 °C under 20% O_2/He for 1 h, and then cooled down to room temperature), and third run (3) (repeat of the second run).

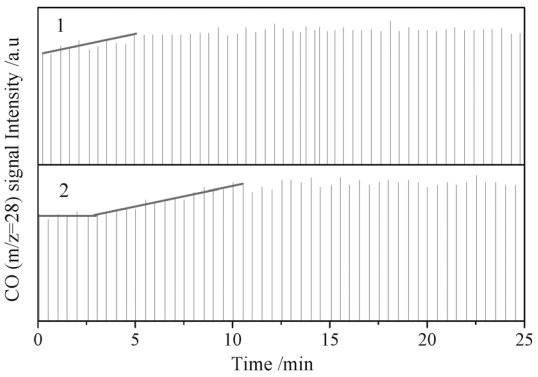

Fig. 8 CO pulse experiment at 60 °C on (1) Cu_1Ce_9–O, (2) $Cu_1Ce_8Fe_1$–O.

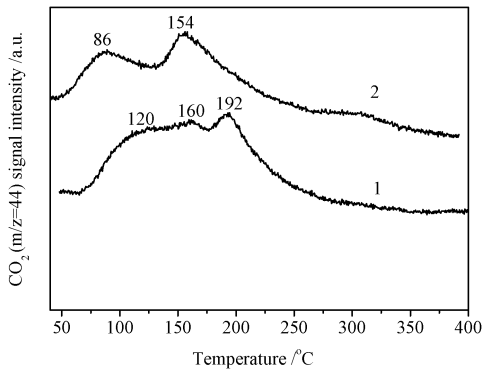

Fig. 9 CO_2 (m/z = 44) evolution curves in CO-TPD-MS of (1) Cu_1Ce_9–O and (2) $Cu_1Ce_8Fe_1$–O.

species to CO_2 at lower temperature than on Cu_1Ce_9–O. This is a reason that the catalytic performance of $Cu_1Ce_8Fe_1$–O is higher than that of Cu_1Ce_9–O for CO oxidation at low temperature.

3.6 Discussion about role of Fe in the Cu–Ce–O catalyst

The testing of the catalytic activities of catalysts (Fig. 1) shows that adding Fe in Cu_1Ce_9–O can improve obviously its catalytic activity for CO oxidation, which can be attributed to following reasons: Firstly, after doping Fe into Cu_1Ce_9–O, the crystallite size of $Cu_1Ce_8Fe_1$–O was decreased from 7.8 nm to 5.2 nm, and its BET surface area was significantly increased from 120 $m^2\ g^{-1}$ to 164 $m^2\ g^{-1}$. Secondly, the surface oxygen species on the $Cu_1Ce_8Fe_1$–O catalyst is much more active than that on Cu_1Ce_8–O, for instance its reduction peak of surface oxygen species (Fig. 6) and its CO_2 desorption peaks (Fig. 9) shift to lower temperature. Also, the amount of surface oxygen species on $Cu_1Ce_8Fe_1$–O is more than that on Cu_1Ce_8–O, for instance the reduction peak intensity of surface oxygen species of $Cu_1Ce_8Fe_1$–O is much stronger (Fig. 6) and the intensities of CO signals (m/z = 28) at the first several pulses on $Cu_1Ce_9Fe_1$–O are lower (Fig. 8) than that on Cu_1Ce_9–O. These may be due to the smaller particle size and higher surface area of $Cu_1Ce_9Fe_1$–O.

The CO pulse experiment (Fig. 8) shows that after the first several pulses, the pulsed CO is mainly converted by the lattice oxygen species migrated from the sub-surface or bulk of catalyst, and the migration rate of lattice oxygen in $Cu_1Ce_8Fe_1$–O is faster than in Cu_1Ce_9–O. The change slope of the CO signals is obviously milder in the spectrum of $Cu_1Ce_9Fe_1$–O than in that of Cu_1Ce_9–O with an increase in the time or pulses of CO, which is induced by different amounts of lattice oxygen or different rates of oxygen migration.

For the CO oxidation over Cu–Ce–O catalyst, there is the Mars–van Krevelen mechanism[9] or Langmuir–Hinshelwood mechanism[32] or both concurrences that the Langmuir–Hinshelwood mechanism was the main reaction mechanism and the Mars–van Krevelen mechanism also existed.[33] We thought[9] the Langmuir–Hinshelwood mechanism may exist as the incidental mechanism in the CO oxidation over the Cu–Ce–O catalyst, and it follows the Mars–van Krevelen mechanism as follows:

$$CO + * \rightarrow CO* \quad (1)$$

$$CO* + O_L \rightarrow COO_L* \quad (2)$$

$$COO_L* \rightarrow * + CO_2 + V_L \quad (3)$$

$$O_2 + V_L \rightarrow 2O_L \quad (4)$$

In eqn (1)–(4), "*" represents an active site, and "O_L" and "V_L" denote the lattice oxygen and oxygen vacancy in the catalyst, respectively. In the $Cu_1Ce_8Fe_1$–O catalyst, the Cu species exists as Cu^+, Cu^{2+} and Cu^0, and among them the Cu^+ has the strongest ability to adsorb CO.[34,35] Ceria has unique oxygen storage properties; adding ceria into CO oxidation catalysts can obviously improve their catalytic performance. When $x \leq 0.2$ $Ce_{1-x}Fe_xO_{2-\delta}$ solid solutions can be formed, and the presence of Fe in CeO_2 can obviously improve the lattice oxygen migration, formation of oxygen vacancies and reducibility of the CeO_2 catalyst, resulting in an increase of its catalytic activity for CO oxidation.[25] Like Ce_9Fe_1–O solid solution, the presence of Fe in $Cu_1Ce_8Fe_1$–O catalyst can improve the lattice oxygen migration, formation of oxygen vacancies and its reducibility, resulting in the acceleration the reactions of eqn (2) and (3).

Conclusions

In summary, the $Cu_1Ce_8Fe_1$–O catalyst has been prepared by improved citrate sol–gel method with incorporation of thermal treatment under N_2, and displays excellent catalytic activity for CO oxidation, T_{90} is 50 °C. Compared with the Cu_1Ce_9–O catalyst, the presence of Fe can increase the surface area of catalyst and diminish the crystalline size. The surface oxygen species on the $Cu_1Ce_8Fe_1$–O catalyst is much more active than that on Cu_1Ce_8–O, and the amount of surface oxygen species on the former is more than that on the latter. The higher catalytic activity of $Cu_1Ce_8Fe_1$–O for CO oxidation is due to its higher surface area and smaller crystalline size, and the more highly active and much larger amounts of the surface active oxygen species on its surface.

Acknowledgements

This project was supported financially by the National Basic Research Program of China (2010CB732300), the Fundamental Research Funds for the Central Universities, and the "Shu Guang" Project (10GG23) and Leading Academic Discipline Project (J51503) of Shanghai Municipal Education Commission and Shanghai Education Development Foundation.

Notes and references

1 J. L. Ayastuy, M. P. Gonzalez-Marcos, J. R. Gonzalez-Velasco and M. A. Gutierrez-ortiz, *Appl. Catal., B*, 2007, **70**, 532–541.
2 Y. H. Wang, J. L. Zhu, J. C. Zhang, L. F. Song, J. Y. Hu, S. L. Ong and W. J. Ng, *J. Power Sources*, 2006, **155**, 440–446.
3 S. Y. Chin, O. S. Alexeev and M. D. Amiridis, *Appl. Catal., A*, 2005, **286**, 157–166.
4 L. H. Chang, N. Sasirekha and Y. W. Chen, *Catal. Commun.*, 2007, **8**, 1702–1710.
5 F. Mariño, C. Descorme and D. Duprez, *Appl. Catal., B*, 2004, **54**, 59–66.
6 C. N. Costa, S. Y. Christou, G. Georgiou and A. M. Efstathiou, *J. Catal.*, 2003, **219**, 259–272.
7 M. F. Luo, J. M. Ma, J. Q. Lu and Y. J. Wang, *J. Catal.*, 2007, **246**, 52–59.
8 J. J. Shao, P. Zhang, X. F. Tang, B. C. Zhang, W. Song, Y. D. Xu and W. J. Shen, *Chin. J. Catal.*, 2007, **28**, 163–169.
9 Y. Liu, C. Wen, Y. Guo, G. Z. Lu and Y. Q. Wang, *J. Phys. Chem. C*, 2010, **114**, 9889–9897.
10 P. G. Harrison, I. K. Ball, W. Azalee, W. Daniell and D. Goldfarb, *Chem. Mater.*, 2000, **12**, 3715–3725.
11 S. Hocevar, U. O. Krasovec, B. Orel, A. S. Arico and H. Kim, *Appl. Catal., B*, 2000, **28**, 113–125.
12 P.-O. Larsson and A. Andersson, *Appl. Catal., B*, 2000, **24**, 175–192.
13 J. Carriazo, E. Guélou, J. Barrault, J. M. Tatibouët, R. Molina and S. Moreno, *Catal. Today*, 2005, **107–108**, 126–132.
14 J. G. Carriazo, L. M. Martınez, J. A. Odriozola, S. Moreno, R. Molina and M. A. Centeno, *Appl. Catal., B*, 2007, **72**, 157–165.
15 Y. P. Hu, H. F. Jin, J. R. Liu and D. S. Hao, *Chem. Eng. J.*, 2000, **78**, 147–152.
16 X. Wang and R. J. Gorte, *Appl. Catal., A*, 2003, **247**, 157–162.
17 I. L. Junior, J. M. M. Millet and M. Aouine, *Appl. Catal., A*, 2005, **283**, 91–98.
18 N. P. Hua, H. T. Wang, Y. K. Du, M. Shen and P. Yang, *Catal. Commun.*, 2005, **6**, 491–496.
19 K. Sekizawa, S. Yano, K. Eguchi and H. Arai, *Appl. Catal., A*, 1998, **169**, 291–297.
20 M. Haruta, N. Yamada, T. Kobayashi and S. Iijima, *J. Catal.*, 1989, **115**, 301–309.
21 B. T. Qiao, L. Q. Liu, J. Zhang and Y. Q. Deng, *J. Catal.*, 2009, **261**, 241–244.
22 L. Liu, F. Zhou, L. Wang, X. J. Qi, F. Shi and Y. Q. Deng, *J. Catal.*, 2010, **274**, 1–10.
23 J. L. Cao, Y. Wang, X. L. Yu, S. R. Wang, S. H. Wu and Z. Y. Yuan, *Appl. Catal., B*, 2008, **79**, 26–34.
24 K. Sirichaiprasert, A. Luengnaruemitchai and S. Pongstabodee, *Int. J. Hydrogen Energy*, 2007, **32**, 915–926.
25 D. S. Qiao, G. Z. Lu, X. H. Liu, Y. Guo, Y. Q. Wang and Y. L. Guo, *J. Mater. Sci.*, 2011, **46**, 3500–3506.
26 M. F. Luo, Y. P. Song, X. Y. Wang, G. Q. Xie, Z. Y. Pu, P. Fang and Y. L. Xie, *Catal. Commun.*, 2007, **8**, 834–838.
27 W. H. Shen, X. P. Dong, Y. F. Zhu, H. R. Chen and J. L. Shi, *Microporous Mesoporous Mater.*, 2005, **85**, 157–162.
28 Hornes, P. Bera, A. L. Camara, D. Gamarra, G. Munuera and A. Martinez-Arias, *J. Catal.*, 2009, **268**, 367–375.
29 X. Q. Wang, J. C. Hanson, A. I. Frenkel, J. Y. Kim and J. A. Rodriguez, *J. Phys. Chem. B*, 2004, **108**, 13667–13673.
30 H. B. Zou, S. Z. Chen and W. M. Lin, *J. Nat. Gas Chem.*, 2008, **17**, 208–211.
31 H. Q. Zhu, Z. F. Qin, W. J. Shan, W. J. Shen and J. G. Wang, *J. Catal.*, 2004, **225**, 267–277.
32 W. Liu and M. Flytzani-Stephanopoulos, *J. Catal.*, 1995, **153**, 317–332.
33 J. B. Wang, D.-H. Tsai and T.-J. Huang, *J. Catal.*, 2002, **208**, 370–380.
34 M. Tada, R. Bal, X. D. Mu, R. Coquet, S. Namba and Y. Iwasawa, *Chem. Commun.*, 2007, 4689–4691.
35 H. Q. Wan, Z. Wang, J. Zhu, X. W. Li, B. Liu, F. Gao, L. Dong and Y. Chen, *Appl. Catal., B*, 2008, **79**, 254–261.

